The microscopic structures for planar and conventional optics, theory and technology

Jan Popelek, František Urban, František Matějka
Department of Microelectronics, Technical University of Brno,
Údolní 53, 602 00 Brno, Czech Republic

1. Introduction

At present, photonic technologies boost most areas of both communication and sensing. Coincidently, most applications of the novel technical solutions based on any sort of optical elements can be found here. Beside the classic bulk optics, there is arising importance of planar and diffractive optics which is able not only to take many typical tasks of the conventional optics over but also to open quite a few new applications. For the planar and diffractive optics is based on the structures of the size comparable to or smaller then a wavelength, it utilises a modern technology, very the same as a semiconductor microelectronics does. One of the technology noticeably used here is an electron beam lithography which allows to generate the dielectric structures with the lateral accuracy up to 0.1 μm or even less. Invented originally for conductive materials the EBL brings some limitations and peculiarities to the fabrication of the dielectric structures like trapped charge effects, proximity effect and others which will be briefly discussed. Most dielectric structures produced by direct EBL are composed of ultra fine relief patterns created either onto the flat bulk wafer surface or onto the layered sandwich substrate. The physical methods of microfabrication allows for getting the reliefs of the depth comparable to the wavelength of light.

2. EBL writing

The essence of the electron writing of microstructures is in physical interaction of incident highly energetic e-beam with matter. In most cases it is the interaction of the electrons with the macromolecules of the polymeric organic thin film. There are two possible ways of changing the properties of the exposed film. The first one, so called positive process, where the energetic electrons break the macromolecules of the organic film and consequently cause the decreasing of the polymer average molecular weight. The second process, the negative one, causes creation of the intermolecular bonds that converts linear molecules into the three dimensional net. The average molecular weight therefore increases. The main representative of the first group is PMMA, the resists which belong to the second group are polysiloxanes. Both the changes of the molecular weight and of the structure reflect into the change of solubility of the resist in an organic solvent (usually a mixture of izobutylketone and izopropanole). The positive resist shows rising solubility starting at some dose of electrons passed through the film. The opposite behaviour is seen in the negative resist group. The writing process would be used:

- to create the masks for further production step (photolithography) which can be used to fabricate the resulting structure,
- to create the technological mask layer for subsequential processing of the same substrate which transfers the pattern from the resist layer to the substrate material,
- to create the functional layer directly into the resist.

In each of these eventualities there are different demands to the resist, namely in terms of its thickness. The last case, where the resist plays the role of the functional layer, would require the resist film thickness being adjusted according to the expected functionality. This pays well for diffractive structures. The requirements vary from 0.1 μm up to several microns. In the two previous items the thickness of the resist film is mostly dictated by the technology.

2.1. Description of EBL writer

In EBL writer, the 15 to 20 keV electrons are formed into the narrow and low numerical apperture gaussian beam. The beam passes through the electrostatic and magnetic lenses, it is magnetically deflected against the rectangular diaphragm and its cross section is shaped into the rectangle of any dimensions from 0.1×0.1 μm to 3×3 μm with the step of 0.1 μm. The shaped beam goes into the deflecting magnetic system and is projected to the mobile table that carries the substrate. Here, the beam writes the pattern having a possibility to be deflected to any of the crossing points of the 32768×32768 line net where the unit length is 0.1 mm (BS 601 apparatus). The exposition

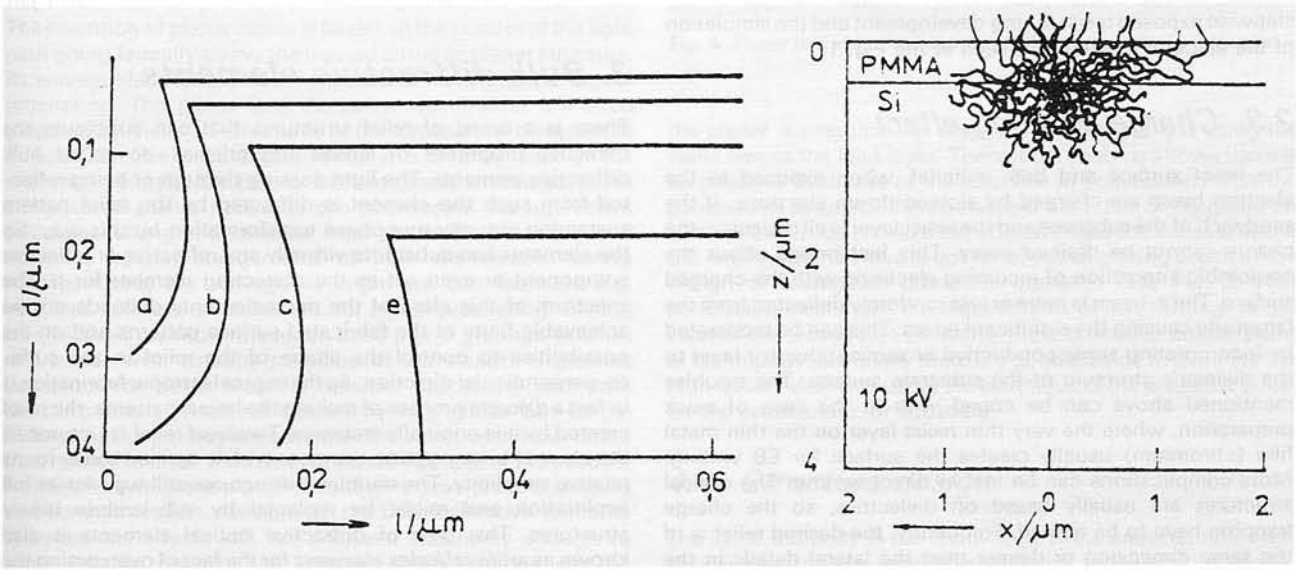

Fig. 1. Proximity effect and electron scattering in the resist

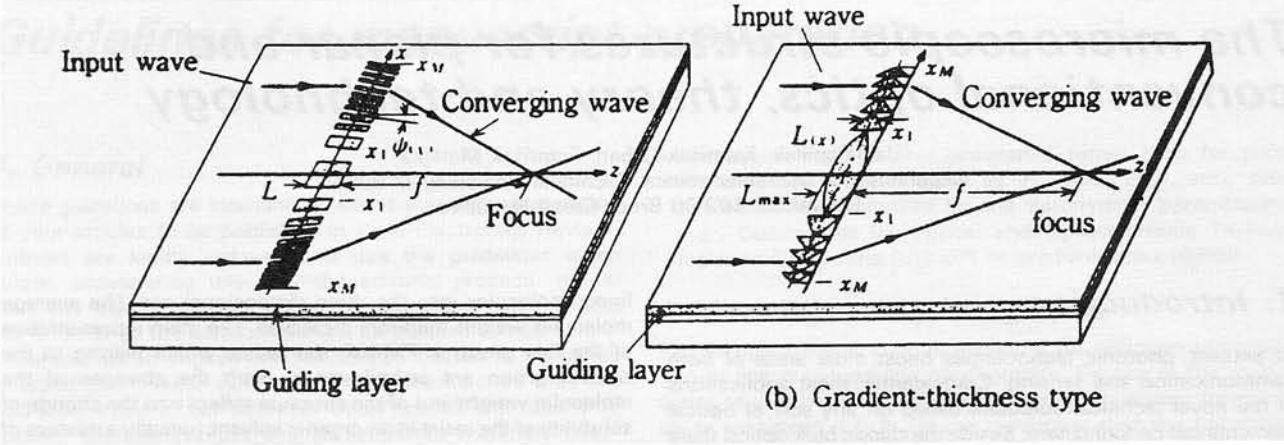

Fig. 2. Guide, refractive and diffractive planar elements

time – the time of radiating at one spot – is controlled by the beam blanking. The pattern is written stamp by stamp with setting the *x–y* position in rectangular coordinates, the rectangular stamp size and the stamp dose for each stamp individually. If needed, the patterns larger than 3.2 × 3.2 mm can be generated by replacing the precisely controlled substrate table whose position is measured using laser interferometers with the accuracy down to 40 nm. Every phase of the writing process cares for keeping the accuracy at the level of geometrical errors, i.e. less than 0.05 μm. So we can generate the patterns with the smallest detail up to 0.1 μm which is of immense importance in the diffractive optics. On the other hand, there are still some factors which can seriously affect the statement above and bring some limitations.

2.2. Proximity effect

The first effect which could seriously cut the wings of the EBL short is the proximity effect. It is based on inevitable scattering of the incident electrons on the atomic structure of both the resist and the substrate. The effect is composed from both the forward and backward scattering. The scattering causes the exposition of the resist in vicinity of the stamped area where the resist surface has not been directly lit. The effect of scattering is random, hence the errors are gaussian. The errors grow with the resist thickness. They can change the shape and the dimensions of the details, especially for the structures tinier than 1 μm and e-beam energy higher than 15 keV. Shape changes of the stepwise exposed resist during development and the simulation of the electron scattering is seen at the Fig. 1.

2.3. Charge trapping effect

The resist surface and bulk material, when exposed to the electron beam are charged by slowed down electrons. If the sandwich of the substrate and the resist layer is all dielectric, the charge cannot be drained away. This fact brings about the coulombic interaction of incoming electrons with the charged surface. The e-beam is more or less randomly deflected from the target site causing the significant errors. This can be moderated by incorporating some conductive or semiconductive layer to the dielectric structure of the substrate surface. The troubles mentioned above can be coped with in the case of mask preparation, where the very thin resist layer on the thin metal film (chromium) usually creates the surface for EB writing. More complications can be met in direct writing. The optical structures are usually based on dielectrics, so the charge trapping have to be treated. Frequently, the desired relief is of the same dimension or deeper than the lateral details in the pattern.

The two ways for fabrication – the resist masking layer and the resist functional layer – have each their own disadvantages. Generally the resist masking layer can be reasonably thin to moderate the proximity effect and, in combination with a conductive layer, the charge trapping effect as well. The developing processes for the resist together with the proximity effect seldom allow the structure detail to be smaller than the thickness of the resist. It should be said, however, that the resist thickness on the flat substrate prepared by spinning off method can be achieved down to 0.1 μm. As successive processes for relief preparation the dry etching or wet anizotropic etching can be used. The first is applicable for virtually all types of substrates. The mask resist is etched simultaneously with the material of the substrate, therefore the deeper groove in the substrate relief than the original resist thickness is hardly achievable. The reactive ion etching applied together with the layered resist is one of the few techniques which offers such the capability. Anizotropic etching is applicable for the monocrystaline substrates, preferably semiconductors. Properly oriented wafer (100 for Si) allows to get highly different etching rates for two main crystal directions. That gives the benefit in etching precisely defined grooves with triangular or trapezium crossections. Their depth can not be higher than the width. If the resist plays the role of the active layer, its thickness is usually determined by the structure design rather than by the technology. Hereabout, preparing the relief patterns, we have to relay on the wet developing process. As a new possibility, we can use the thermal collapse of the exposed resist. Still, both of the techniques are scarcely usable for the relief deeper than 1 μm.

3. Bulk diffractive elements

There is a breed of relief structures that can substitute the refractive properties of lenses and prismas, so called bulk diffractive elements. The light passing through or being reflected from such the element is diffracted by the relief pattern sustaining virtually any phase transformation by this way. So the elements can substitute virtually any refractive or reflective component or even act as the correcting member for it. The spectrum of this class of the microelements depends on the achievable finity of the fabricated surface patterns and on the possibilities to control the shape of the relief in the surface-perpendicular direction. As the microelectronic fabrication is in fact a discrete process of making the lateral patterns, the relief created by it is originally stepwise. Twolevel relief structures fill the class of binary optics, the most widely applied today for its relative simplicity. The multilevel structures still wait for its full exploration and might be replaced by sub-lambda binary structures. This type of diffractive optical elements is also known as *artificial index elements* for the fact of overcoming the limitation in the number of feasible phase-shift levels by

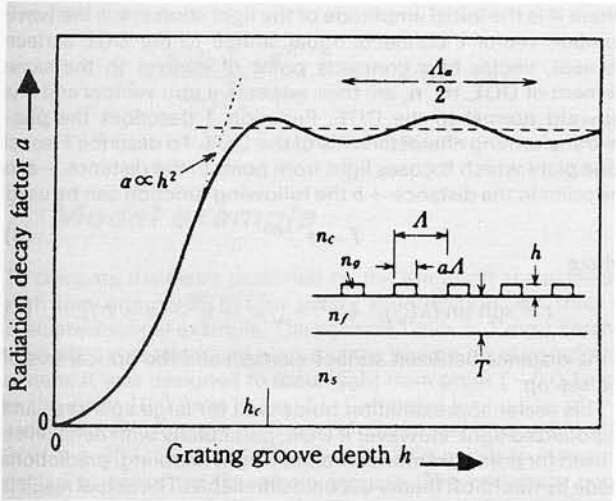

Fig. 3. Effective groove depth for planar gratings

creation of tiny structures below the wavelength. This kind of microstructures can simulate the continuous change of index of refraction in the optical element. These dielectric microstructures have generally very deep relief and they are more sensitive to proper design. Their strong influence to the polarization state of the diffracted light brings new difficulties to the whole process of diffractive element design.

In this class of the optical microstructures there are various requirements for the technology. Binary elements need the relief structures with the optical path step of $\lambda/2$. This corresponds to the depth of the relief about $\lambda/4$ where using the reflective surface and $\lambda/2$ for SiO_2 or the developed resist layer on the flat reflector. The transmissive arrangement of the structure needs relief about λ deep. Those demands can be adopted by the EBL technology quite well for UV up to NIR light. Higher wavelength elements can be realized more easily by use of the artificial index structures where subwavelength tiny and deep notches in the highly refractive material substitute an index drop. Controlling both the density and the width of the notches it is possible to change the refractive properties of the layer, provided the mean period of the notches is by an order higher than the wavelength. This type of the structures can be realized by selective dry etching of masked high refractive material like Si_3N_4 for visible or Si and GaAlAs for IR radiation.

4. Planar optics

The invention of planar optics is based on the control of the light path going laterally throw the layered stripe or planar structure. Its waveguide origin, is currently used in many tasks of signal processing. The planar and the stripe waveguides are often prepared by the relief structures of the dimensions comparable or less then the wavelength, hence it is also the task of the microtechnologies like EBL to fabricate these structures. Quite complicated planar networks can acomodate the equivalent principles taking the essence from the bulk diffractive and refractive optical arangements or from the electric wiring models. Using the waveguide origin we can fabricate e.g. couplers, splitters, switches etc. for signal processing. Basing on effective index control we can build planar gratings, prismas and lenses with virtually any kind of wavelength-dispersive behaviour for beam shaping, spectral processing and path directing. These structures operate by very similar way as the bulk ones, except they are based on the effective indices rather then refractive ones. Also here, there are a couple of the peculiar features for which the planar circuits gets more place in sensing and communication. Similarly to the bulk diffractive elements there are the effects still not analyzed accurately enough to allow reliable design. The effective index change can be arranged by the load layer deposited onto the guiding layer of

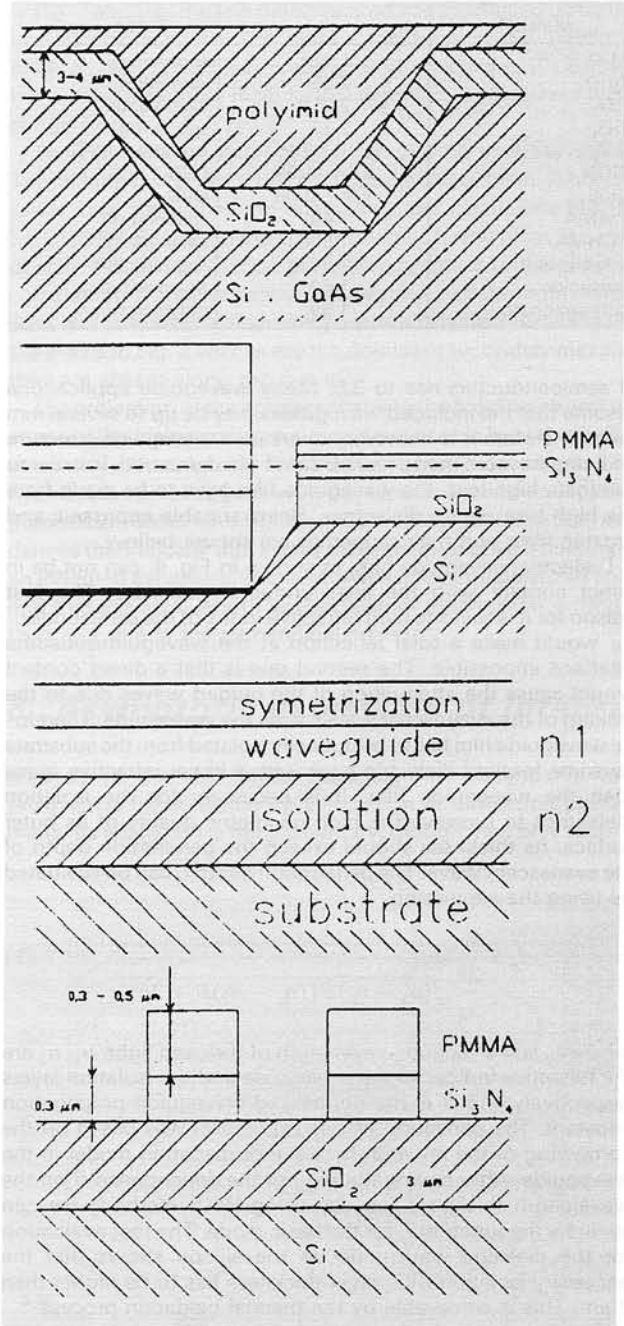

Fig. 4. Planar and stripe waveguide on the semiconductor substrate

the planar waveguide. An easy way for doing this is using the resist film as the load layer. Theoretical analysis shows there is an effective thickness of the load film in coincidence with the penetration length of the evanescent field. For Si_3N_4 guide on silica or oxinitride on silica the effective load thickness is about 0.2 μm. The same value is got for effective grating depth in the design of waveguide diffractive elements (see Fig. 3. That conclusion meets well the requirements of EBL writing. In the class of the waveguide elements, there is another crucial point of technology. Generally there is a good chance to fabricate the high quality elements using the technique of the dielectric guide on the semiconductor substrate.

4.1. Structure design

The initial difficulty in the technology is the unacceptable high optical loss and the very high refractive index of Si or GaAs. Typically, observed loss exceeds 20 dB cm^{-1}. Refractive index

Material	nr	Technology
Al_2O_3	1.624	sputtering
Ta_2O_5	2.05	sputtering
TiO_2	2.21	evaporation
TiO_2	2.37	sputtering
SiO_2	1.40÷1.45	oxidation, CVD
SiON	1.48÷1.99	CVD
Si_3N_4	1.90÷2.05	CVD
PMMA	1.49	spinning off
PCHMA	1.505	spinning off
polystyrene	1.58	spinning off
polyimide	1.60	polymerization
polycarbonate	1.59	polymerization

of semiconductors rise to 3.5. Many waveguide applications assume that the included waveguides may be up to several mm long. Therefore it is necessary to create a waveguide structure showing no more then a few dB cm^{-1} of attenuation. In order to eliminate high loss, the waveguide film have to be made from the high transparent dielectrics. Some suitable anorganic and organic films and their properties are shown bellow.

Dielectric waveguide film, as shown in Fig. 4, can not be in direct contact with the semiconductor substrate. The first reason for it is that the high refractive index of the semiconductor would make a total reflection at the waveguidesubstrate interface impossible. The second one is that a direct contact would cause the attenuation of the guided waves due to the leaking of the evanescent waves from the waveguide. Therefore, waveguide film has to be optically isolated from the substrate by some lossless dielectric layer with a lower refractive index then the waveguide film. It is necessary for the isolation dielectrics to preserve the high geometric quality of its outer surface. Its thickness should exceed the penetration depth of the evanescent wave. The penetration depth l_p can be evaluated by using the expression

$$l_p = \frac{1}{\frac{2\pi}{\lambda_0}\sqrt{(n_1 - n_2)B[(n_1 - n_2)B + 2n_1]}} \tag{1}$$

where λ_0 is the vacuum wavelength of the used light, n_1, n_2 are the refractive indices of the waveguide and the isolation layers respectively and B is the normalized waveguide propagation constant. The derivation of this expression was based on the combining of the ray and the wave propagation model in the waveguide. After having figured out the dependence B on the wavelength thickness (i.e., by using WKB method) we can evaluate the function l_p for the basic mode. The loss evaluation for the dielectic waveguide on the silicon shows that the necessary isolation SiO_2 layer thickness has to be higher than 3 μm. This is achievable by the thermal oxidation process.

As we can see, both planar and bulk diffractive optics are tightly bond to precisely designed diffractive microstructures. Except of regular gratings the theory of wave interaction with near-lambda microstructures is in its cradle. Present state-ofart in this field is totaly wretched. Discussing the range of the features of the diffractive elements we would like to point out their sensitivity to the state of polarisation of the incident light. Their behaviour and the importance of the polarisation state to the effective/refractive indices can affect the very operability of some diffractive elements and has not been studied yet.

5. Scalar theory of diffraction

The current DOE design technology is based on Kirchhoff scalar theory of diffraction. It has been derived from the Green integral theorem for two scalar functions inside and on a closed surface. Assuming point source of light the amplitude of the diffracted light U_P behind the phase-transforming DOE can be formulated by following equation

$$U_P = -\frac{ikA}{4\pi}\oint_S T\frac{e^{ik(r+s)}}{rs}(\mathbf{n}\mathbf{n}_s - \mathbf{n}\mathbf{n}_r)\,dS, \tag{2}$$

where A is the initial amplitude of the light source, k is the wave number, vector **r** connects initial source to the DOE surface element, vector bf s connects point of interest to the same element of DOE, $\mathbf{n}_r$, $\mathbf{n}_s$ are their respective unit vectors and n is outward normal to the DOE. Function T describes the phase-transforming characteristics of the DOE. To describe Fresnel zone plate which focuses light from point in the distance $-a$ to the point in the distance $+b$ the following function can be used

$$T = e^{-i\pi t}, \tag{3}$$

where

$$t = \mathrm{sgn}\sin\left[k\left(\sqrt{\rho^2 + a^2} + \sqrt{\rho^2 + b^2} - a - b\right)\right], \tag{4}$$

is the distance between surface element and the optical axis of the set-up.

This scalar approximation holds well for large apertures and unpolarized light. However if DOE, particularly with deep relief, is used for polarized monochromatic light handling, predictions made by Kirchhoff theory become unreliable. The actual result is not invariant to the rotation of polarization plane in contrast to the theoretical evaluation of this problem.

6. Vector modification of Huygens-Fresnel principle

Our attemp to overcome these limits in correct assessment of light – DOE interaction is based on *modified* Huygens-Fresnel principle:

Every point of a wave-front can be considered to be an elementary dipole emanating electromagnetic radiation. The wave-front at any later instant may be regarded as the mutual interference field of these wavelets.

Thus, in our modification the term *electric dipole* replaces the original term *elementary light source*.

The field radiated by an elementary dipole is rigorously described by the equation

$$\mathbf{E} = \frac{e^{ikR}}{4\pi\varepsilon_0 R}\left\{\frac{(\mathbf{p}_0\mathbf{R})\mathbf{R}}{R^2}\left(\frac{3}{R^2} - \frac{3ik}{R} - k^2\right) - \mathbf{p}_0\left(\frac{1}{R^2} - \frac{ik}{R} - k^2\right)\right\}. \tag{5}$$

$$\mathbf{H} = \frac{e^{ikR}}{4\pi R}\left\{\frac{-ik}{R} - k^2\right\}\frac{\mathbf{p}_0 \times \mathbf{R}}{R}. \tag{6}$$

For the sake of simplicity let us abandon the small contribution to the overall field amplitude

$$k^2 \gg \frac{k}{R} \gg \frac{1}{R^2}. \tag{7}$$

After simplification the total field amplitude at point P is

$$\mathbf{E}_P = \frac{k^2}{4\pi\varepsilon_0}\oint_S \frac{e^{iks}}{s}\left\{\mathbf{p}_0 - \frac{(\mathbf{p}_0 S)S}{s^2}\right\}dS. \tag{8}$$

Let us assume again, that the only source of light is a solitary dipole placed in the distance $-$a. The second assumption is linear dependency $\mathbf{p} = C\mathbf{E}$. Substituing into equation 8 we obtain after some calculation

$$\mathbf{E}_P = \frac{C^2k^2E_0}{16\pi^2\varepsilon_0^2}\oint_S T\frac{e^{ik(r+s)}}{rs}\{[\mathbf{n}_{E_0} - (\mathbf{n}_{E_0}\mathbf{n}_r] - \\ - \{[\mathbf{n}_{E_0} - (_{E_0}\mathbf{n}_r)\mathbf{n}_r]\mathbf{n}^s\}\mathbf{n}_s\}\,dS. \tag{9}$$

Unit vectors $\mathbf{n}_X$ denote the direction of their respective counterparts **X**. Equation 9 is the vector equivalent to the equation 2 and we use this fact for the zero aproximation to the constant C. To maintain the same numeric value of both integrals we have choosen the constant C to satisfy equation

$$C = \frac{\varepsilon_0}{k}\sqrt{-2\lambda i}. \tag{10}$$

The final formula is

$$\mathbf{E}_P = \frac{ik^2 E_0}{4\pi} \oint_S T \frac{e^{ik(r+s)}}{rs} \{[\mathbf{n}_{E_0} - (\mathbf{n}_{E_0}\mathbf{n}_r] - - \{[\mathbf{n}_{E_0} - (_{E_0}\mathbf{n}_r)\mathbf{n}_r]\mathbf{n}_s\}\mathbf{n}_s\} \, dS. \quad (11)$$

7. Model example

To compare the result predicted by the Kirchhoff scalar theory with that one given by our vector modification, we tried to evaluate a simple example. The squaare(1 mm × 1 mm) Fresnel zone plate was taken and placed at the beginning of coordinate system. It was designed to focus light from point [−0,0,1mm] to the point [0,0,2mm] (Fig. 5). Computer evaluation of this problem took about 120 hours of computer time (IBM-PC, 386SX + 387, 25 MHz). We used 10 PCs mutually interconnected to speed up the whole process. The necessary computing time restricted the maximum dimension of the evaluated Fresnel zone plate. A simple calculation of computing time for bigger lenses convinced us that this task can not be solved by use of brutal force.

Fig. 6 and Fig. 8 show the intensity profile calculated using equation 2. The displayed area is a square 10 μm × 10 μm. We can see the symetricity of the profile. The dimensions of the central maximum are about 3.5 μm × 3.5 μm.

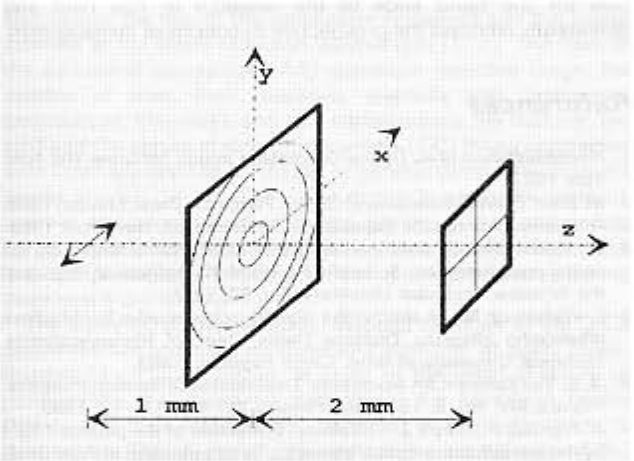

Fig. 5. Model example set-up

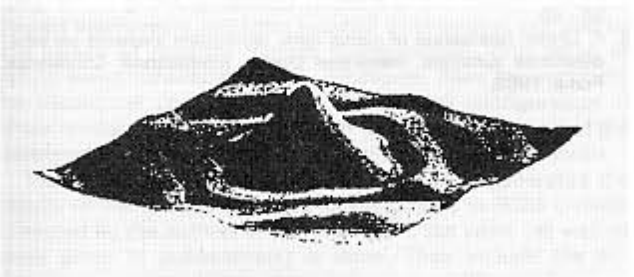

Fig. 6. Intensity profile calculated by the scalar theory

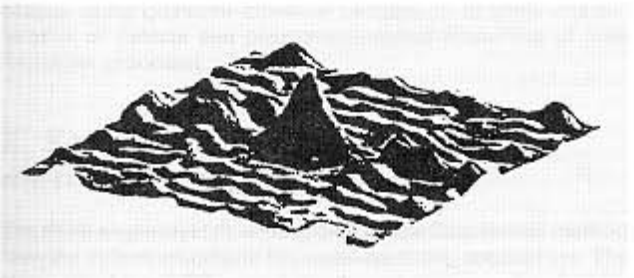

Fig. 7. Intensity profile calculated by the vector modification

Fig. 7 and Fig. 9 show the same area, but calculated using our vector modification. The source electromagnetic dipole is oriented along the x-axis of the coordinate system. We can see the central maximum is no longer symetric, its dimensions are about 2.5 μm × 1.5 μm.

There are peculiar rectangular paterns visible on these figures. The striking fact is totaly different orientation of them. While the scalar case has a rhombic orientation, the vector one has the barier perpendicular to the aperture edges. It resembles to a kind of scaled-down projection of the lens aperture to the plane of calculation. The significantly different shape of the main central peak is clearly visible. Following the intensity distribution along the x-axis in Fig. 7 we can see the dominant secondary maxima; they are absent along the y-axis.

The projection of the aperture shape to the focal plane and the shape of the main maximum support reasonable hypothesis that there are different focal lengths for x and y-directions. This hypothesis complies both with the experiment and an intuitive theoretical model of diffraction. Our vector modification evidences theoretically that axially symetric diffractive lenses have an inherited astigmatic aberation when focusing polarized light and that the focal length in the plane of polarization is longer than that one in the perpendicular plane.

8. Asymptotic expansion of integral

Method of the asymptotic expansion of integrals is very prospective for speeding up calculation of diffraction phenomena. Its aplication is not elementary, though. Not only there is

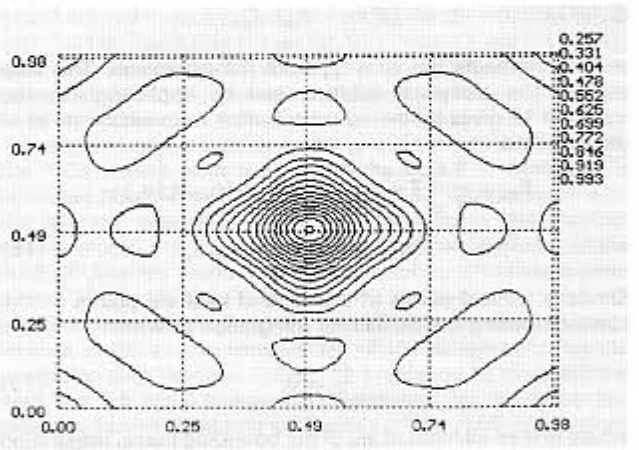

Fig. 8. The topographic map of the scalar intensity profile

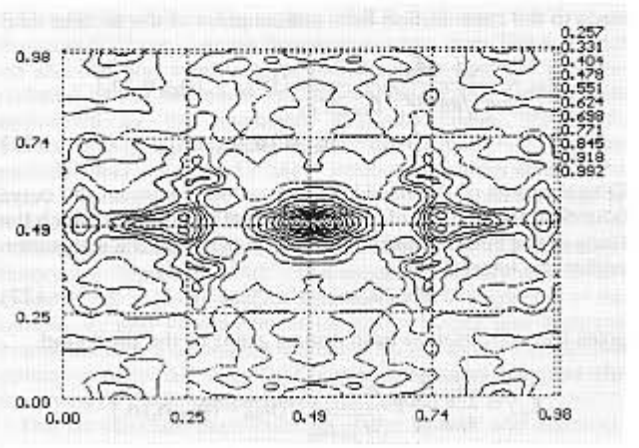

Fig. 9. The topographic map of the vector intensity profile

a need for quite complex mathematic aparatus, but also there are omittings and mistakes at the papers of foundators of its method. The extremaly good feature of this method is that it complexity and computer time requirement are not depending on the size of DOE. The method consists in replacement of whole integral by sum of only few contributions that arise from certain specially chosen critical points. Evaluation of the integral

$$\iint g(x, y) e^{ikf(x,y)} dx\, dy \tag{12}$$

starts with expansion of the phase function f into the series

$$f(x, y) = f_{00} + f_{10}(x-x_0) + f_{01}(y-y_0) + \frac{1}{2} f_{20}(x-x_0)^2 + $$
$$+ f_{11}(x-x_0)(y-y_0) + \frac{1}{2} f_{02}(y-y_0) + \ldots, \tag{13}$$

where

$$f_{ab} = \frac{\partial^{a+b} f(x_0 \cdot y_0)}{\partial x^a \partial y^b} \tag{14}$$

A critical point of the first kind is a point within the domain of integration at which

$$\frac{\partial f}{\partial x} = \frac{\partial f}{\partial y} = 0, \tag{15}$$

Because only small area around this critical point has significant influence to the sum and contributions from others points are efectively canceled, we can integrate inside the interval

$$x \in \langle -\infty, \infty \rangle;\ y \in \langle -\infty, \infty \rangle. \tag{16}$$

Now we transform the coordinate system. Using rotation with angle α,

$$\mathrm{tg}\,(2\alpha) = \frac{f_{11}}{f_{20} - f_{02}}, \tag{17}$$

we can eliminate the term f_{11} from the expansion. This step enables the analytical solution and its application to the equation 11 gives following contribution from critical point of the first kind

$$\mathbf{E}_{P1} = \frac{1}{4} \frac{E_0}{rs} T \frac{e^{ik(r+s)}}{\sqrt{f'_{20} f'_{02}}} \{[\mathbf{n}_{E0} - (\mathbf{n}_{E0}\, \mathbf{n}_r)\mathbf{n}_r] - $$
$$- \{[\mathbf{n}_{E0} - (\mathbf{n}_{E0}\, \mathbf{n}_r)\mathbf{n}_r]\mathbf{n}_s\}\mathbf{n}_s\}. \tag{18}$$

Similarly, critical points of the second kind are points on the curve bounding the domain of integration at which

$$\frac{\partial f}{\partial l} = 0, \tag{19}$$

where dl is an element of arc of the bounding curve. Integration inside the interval

$$x' \in \langle 0, \infty \rangle;\ y' \in \langle -\infty, \infty \rangle. \tag{20}$$

leads to the contribution from critical point of the second kind

$$\mathbf{E}_{P2} = \frac{\sqrt{i}}{4\sqrt{k\pi}} \frac{E_0}{rs} T \frac{e^{ik(r+s)}}{f'_{10}\sqrt{f'_{02}}} \{[\mathbf{n}_{E0} - (\mathbf{n}_{E0}\, \mathbf{n}_r)\mathbf{n}_r] - $$
$$- \{[\mathbf{n}_{E0} - (\mathbf{n}_{E0}\, \mathbf{n}_r)\mathbf{n}_r]\mathbf{n}_s\}\mathbf{n}_s\}, \tag{21}$$

Critical points of the third kind are corner points on the curve bounding the domain of integration, that is, points at which the slope of the curve is discontinuous. In this case the integration within the interval

$$x' \in \langle 0, \infty \rangle;\ y' \in \langle 0, \infty \rangle. \tag{22}$$

gives the contribution from critical point of the third kind

$$\mathbf{E}_{P3} = \frac{i}{4k\pi} \frac{E_0}{rs} T \frac{e^{ik(r+s)}}{\sqrt{f'_{10} f'_{01}}} \{[\mathbf{n}_{E0} - (\mathbf{n}_{E0}\, \mathbf{n}_r)\mathbf{n}_r] - $$
$$- \{[\mathbf{n}_{E0} - (\mathbf{n}_{E0}\, \mathbf{n}_r)\mathbf{n}_r]\mathbf{n}_s\}\mathbf{n}_s\}. \tag{23}$$

Due to the function T the subintegral function is not continuous within the integration domain, this fact breaks the conditions of this method. Dividing the whole domain to zones with constant phase shift we can fulfill these conditions. Each zone of the DOE will be therefore computed separately and the total effect will be summed. Thus the necessary computing time is dependent only to the number of Fresnel zones in the zone plate which increases with the d/f ratio and not with the size of the element.

To compare the significant difference between diffraction patterns predicted both by Kirchhoff scalar theory and modified Huygens-Fresnel principle we are currently evaluating simple optical element using both theories. The final judgement will be naturaly made by measurement of element optical properties. Taking into account the required precision of measured values, we decided to design, produce, compute and measure a relatively simple dielectric grating fabricated of the PMMA layer 0.628 μm thick placed on the silica vafer. The periode of the grating is 1.2 μm, the distance between two ridges is 0.6 μm . The grating is windowed by the square aperture 3×3 milimetres and was designed for operation with red He-Ne laser. Computational study of polarized light interaction with this test grating is carried out using computer DEC system 5100 running exclusively first version of our C-language program. The software for diffraction simulation will be tested in both full an assymptotic version.

The mutual comparison of results obtained by several very different methods should bring new light to the problem of diffractive phenomena on deep dielectrical microstructures, cuts off the blind ends of the research in this field and definiteluly ilmitates the prospective directions of investigation.

References

1. *Hiroshinishihara et al.*: Optical Integrated Circuits. McGraw-Hill, New York 1987.
2. *M. Born, E. Wolf*: Principles of Optics. Pergamon Press, London 1959.
3. *A. Erdéilyi*: Asymptotic Expansions. McGraw-Hill, New York 1956.
4. *G. Mulak*: Metoda stacjonarnej fazy w oszacowaniu amplitudy fali ugijtej przez hologram. Scientific Papers of the Institute of Physics of the Wroclaw Technical University, No. 30, 1991.
5. *L. Vřeštálová*: Návrh efektivniho výpočtu zobecněného Kirchhoffova difrakčniho integrálu, Diploma Thesis, Dept. of Microelectronics, Technical University of Brno, Czech Republic, 1993.
6. *N. G. Van Kampen*: An Asymptotic Treatment of Diffraction Problems. Physica XIV, No. 9, 1949, and Physica XVI, No. 11–12, 1950.
7. *J. Popelek, F. Urban, L. Vřeštálová*: Diffraction of the polarized light by the real diffractive optical elements. To be published in *Proc. SPIE*, Vol. 1991.
8. *F. Urban and F. Matějka*: Planar Diffractive Optical Elements Prepared by Electron-Beam Lithographyin, *Proc. SPIE*, Vol.1574, 1991, pp. 58–65.
9. *F. Urban*: Realisation of planar optic waveguide elements on semiconductor substrate. Integrated Optics, International Conference, Praha, 1989.